WATER RESOURCES RESEARCH, VOL. 49, 4730–4737, doi:10.1002/wrcr.20376, 2013

Hydraulic conductivity fields: Gaussian or not?

Mark M. Meerschaert,[1] Mine Dogan,[2] Remke L. Van Dam,[2] David W. Hyndman,[2] and David A. Benson[3]

Received 5 January 2013; revised 7 June 2013; accepted 17 June 2013; published 5 August 2013.

[1] Hydraulic conductivity (K) fields are used to parameterize groundwater flow and transport models. Numerical simulations require a detailed representation of the K field, synthesized to interpolate between available data. Several recent studies introduced high-resolution K data (HRK) at the Macro Dispersion Experiment (MADE) site, and used ground-penetrating radar (GPR) to delineate the main structural features of the aquifer. This paper describes a statistical analysis of these data, and the implications for K field modeling in alluvial aquifers. Two striking observations have emerged from this analysis. The first is that a simple fractional difference filter can have a profound effect on data histograms, organizing non-Gaussian ln K data into a coherent distribution. The second is that using GPR facies allows us to reproduce the significantly non-Gaussian shape seen in real HRK data profiles, using a simulated Gaussian ln K field in each facies. This illuminates a current controversy in the literature, between those who favor Gaussian ln K models, and those who observe non-Gaussian ln K fields. Both camps are correct, but at different scales.

Citation: Meerschaert, M. M., M. Dogan, R. L. Van Dam, D. W. Hyndman, and D. A. Benson (2013), Hydraulic conductivity fields: Gaussian or not?, *Water Resour. Res.*, *49*, 4730–4737, doi:10.1002/wrcr.20376.

1. Introduction

[2] Groundwater flow and transport simulations require a densely defined hydraulic conductivity (K) field to populate the model grid. Because it is not practical to collect 2-D or 3-D data at this resolution, stochastic simulation methods are commonly used to interpolate between measured data values. Stochastic K field simulation requires a statistical analysis of the available K data, to ensure that the synthesized K field resembles the data in terms of its distribution and correlation structure. The two main simulation steps are: (1) generate an uncorrelated noise field and (2) apply an appropriate filter to impose a correlation structure. Since random number generators produce only uncorrelated noise, both steps are necessary. To parameterize the simulation model, the process is reversed: (1) apply an appropriate inverse filter to the raw data to remove the correlation and (2) examine the filtered, uncorrelated data to determine its true underlying distribution. Unless the data is filtered properly to remove correlations, the data histogram can significantly misrepresent the underlying distribution, since a histogram of correlated data need not reflect the true underlying distribution. In this paper, we will see a remarkable example of this simple and well-known fact.

[3] Hydraulic conductivity data from the Macro Dispersion Experiment (MADE) site, at the Columbus Air Force Base in Mississippi, clearly show a high level of heterogeneity [*Rehfeldt et al*., 1992; *Zinn and Harvey*, 2003; *Llopis-Albert and Capilla*, 2009]. The site was recently revisited to obtain K measurements with much higher spatial resolution than previous measurements [*Bohling et al*., 2012; *Liu et al*., 2009]. Vertical columns (profiles) of hydraulic conductivity data were measured at approximately 1.5 cm depth increments, using a new direct-push profiling method that couples the direct-push injection logger (DPIL) and the direct-push permeameter (DPP) [*Butler et al*., 2007; *Liu et al*., 2009, 2012]. This novel high-resolution K (HRK) tool was advanced into the subsurface, while water was injected out of a small screened port located a short distance behind the tool tip. The injection rate, and injection-induced back pressure, were recorded every 1.5 cm, and the ratio of these quantities was then transformed into K estimates [*Liu et al*., 2009]. The cm-scale spatial resolution of the resulting K data is orders of magnitude finer than the data considered in previous studies [*Rehfeldt et al*., 1992; *Meerschaert et al*., 2004]. *Bohling et al*. [2012] analyzed the resulting K data, and compared those measurements to previous flowmeter-based K estimates collected at lower resolution across the same site.

[4] A parallel data collection effort used ground-penetrating radar (GPR) to image the related sedimentary structures in the aquifer, called facies, by identifying distinct reflection characteristics, such as reflection terminations, dip angles, amplitudes, and continuity. Such GPR facies have been shown to correlate with hydrogeological units [*Van Overmeeren*, 1998; *Heinz and Aigner*, 2003; *Schmelzbach et al*., 2011]. Full-resolution 3-D GPR data using 50 and 100 MHz antennae were obtained with step sizes (and line spacings) of 0.2 and 0.1 m, respectively,

[1]Department of Statistics and Probability, Michigan State University, East Lansing, Michigan, USA.
[2]Department of Geological Sciences, Michigan State University, East Lansing, Michigan, USA.
[3]Hydrologic Science and Engineering, Colorado School of Mines, Golden, Colorado, USA.

Corresponding author: M. M. Meerschaert, Department of Statistics and Probability, Michigan State University, East Lansing, MI 48824, USA. (mcubed@stt.msu.edu)

0043-1397/13/10.1002/wrcr.20376

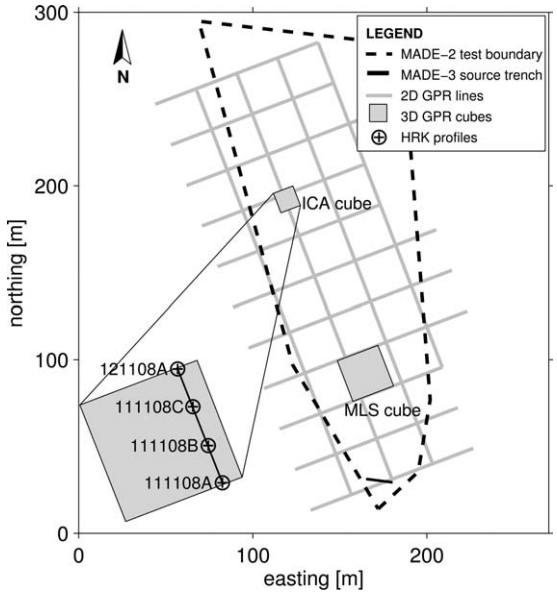

Figure 1. Layout of Macrodispersion Experiment test site, showing key features of MADE-2 and MADE-3 experiments, as well as the locations of GPR data collected for this project. The inset of the 12 × 12 m ICA (Intensively Cored Area) cube shows the locations of the four HRK profiles and the 2-D transect discussed in this paper.

using a Sensors and Software pulseEKKO 100 system. Data processing and analysis to extract facies boundaries were detailed in *Dogan et al*. [2011]. The map in Figure 1 outlines the GPR data collection site, and the location of the four HRK profiles that form the basis for our study. The intensively cored area (ICA) cube was the site of a push-pull tracer test described in *Liu et al*. [2010], see also *Zheng et al*. [2011]. The multilevel sampler (MLS) cube was the site of the MADE-5 tracer test reported in *Bianchi et al*. [2011].

[5] The modeling of hydraulic conductivity fields at the MADE site has been the focus of intensive study and modeling for over 20 years. The geostatistical analysis of *Rehfeldt et al*. [1992] documented a high level of heterogeneity, indicated by the variance of 4.5 for ln K in their multi-Gaussian model, as well as anisotropy, indicated by horizontal and vertical correlation scales of 12.8 and 1.6 m, respectively. *Silliman and Wright* [1988] and *Rubin and Journel* [1991] argued that a Gaussian model with a single covariance function cannot reproduce the preferential pathways (connected regions with the highest ln K values) observed in real aquifers. *Gómez-Hernández and Wen* [1998] continued this argument against the multi-Gaussian model, and cautioned against drawing broad conclusions on the basis of one-dimensional data distributions. *Renard and Allard* [2011] survey several methods for characterizing connectivity, and note that the multi-Gaussian model alone is often insufficient to reproduce the connectivity observed in real aquifers. Significant deviations from a Gaussian profile were noted by *Painter* [1996] and *Meerschaert et al*. [2004], and some alternative non-Gaussian models were proposed. *Zinn and Harvey* [2003] point out that even in a model with Gaussian ln K profiles, deviation from the usual multi-Gaussian model can lead to connected features. *Salamon et al*. [2007] discuss the non-monotone variograms in MADE ln K data, and recommend a sequential Gaussian simulation methodology with a non-monotone covariance structure, to reproduce this "hole effect." *Llopis-Albert and Capilla* [2009] use a gradual conditioning algorithm to produce non-Gaussian ln K fields based on flowmeter, head, and concentration data from MADE-2. This controversy between Gaussian and non-Gaussian ln K fields has profound implications for flow and transport modeling. Heavy tailed ln K distributions support novel approaches including the continuous time random walk (CTRW) [*Berkowitz et al*., 2006], fractional advection dispersion equation (ADE) [*Benson et al*., 2013], and some related stochastic hydrology models [*Cushman and Ginn*, 2000; *Neuman and Tartakovsky*, 2009], while Gaussian ln K models are more consistent with the traditional ADE, mobile-immobile, and dual-domain models.

[6] The two main findings of this study are that: (1) a fractional difference filter can be useful to reveal the true underlying distribution of highly correlated vertical columns of HRK data and (2) using GPR facies, a multi-Gaussian simulation method with an appropriate operator scaling correlation structure applied to each facies can reproduce the significantly non-Gaussian profiles seen in columns of filtered HRK data. There remains a significant debate in the literature between those who favor Gaussian models, and others who believe that a non-Gaussian approach is needed. In our view, both groups are correct, albeit at different scales. Within a single facies, an appropriate multi-Gaussian model can be effective, and when different facies are combined, a non-Gaussian profile with a sharper peak and a heavier tail will emerge.

2. Statistical Analysis

[7] Many studies have analyzed the statistical properties of low-resolution K data profiles; see *Meerschaert et al*. [2004] for a brief review. A typical field experiment collects K data at a vertical resolution of 1−3 m. Since the vertical resolution of the new HRK data is orders of magnitude finer, it is useful to reconsider the results of past analyses. For relatively homogeneous aquifers, it has been common to employ a log-normal distribution for K: the distribution of ln K is assumed to be normal, and aquifer heterogeneity is inferred from the variance of ln K [*Rehfeldt et al*., 1992]. A more detailed analysis suggests a departure from normality, with a sharper peak and heavier tails [e.g., *Lu et al*., 2002; *Meerschaert et al*., 2004]. This deviation becomes more significant for aquifers that display a higher degree of heterogeneity.

[8] Typical values for ln K are highly correlated, leading many researchers to employ models such as a fractional Brownian motion. The MADE site is highly heterogeneous, with ln K variance greater than 4.5. Several novel models have been proposed to try and capture this combination of non-Gaussian distributions and strong correlations [e.g., *Painter*, 1996; *Herrick et al*., 2002; *Molz and Boman*, 1993; *Kohlbecker et al*., 2006].

[9] Figure 2a shows a histogram of ln K data from HRK profile 121108A (see map in Figure 1). The histogram suggests a complex underlying distribution, widely varying with several peaks, and no simple discernible shape. A

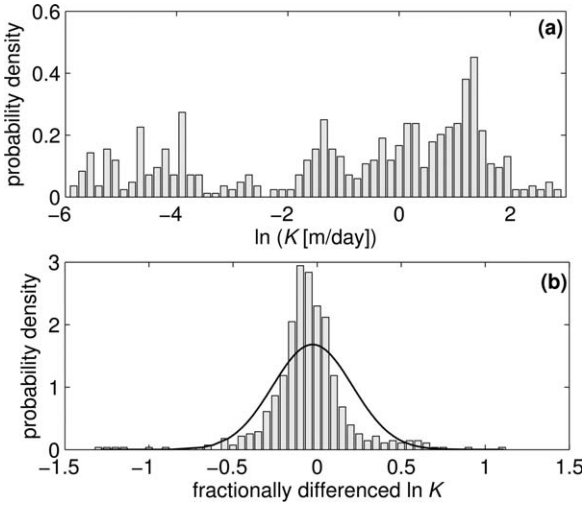

Figure 2. Histogram of ln K for HRK profile 121108A (see map in Figure 1) (a) before and (b) after applying the fractional difference filter equation (1) with $d = 0.9$. The filtered data are organized into a unimodal distribution with a sharper peak and a heavier tail than the best fitting Gaussian pdf (black line).

fractional difference filter was applied to remove the correlations, resulting in the histogram in Figure 2b. The filtered data show no significant serial correlations, indicating that fractionally integrated noise is a reasonable model for this vertical column of ln K data. Fractional models have been applied in hydrology since pioneering work of *Hurst* [1951] on flood levels of the Nile river. In these models, observations X_n are related to a sequence of independent and identically distributed random variables Z_n (white noise) by the fractional difference relation

$$Z_n = \sum_{j=0}^{\infty} w_j X_{n-j}, \tag{1}$$

where the fractional binomial coefficients w_j can be computed recursively using $w_0 = 1$ and $w_j = w_{j-1}(j - 1 - d)/j$ for $j \geq 1$. If the underlying noise sequence Z_n is Gaussian, then the sequence X_n is a fractional Brownian motion with Hurst index $H = d - 1/2$. See Appendix A for more details.

[10] Figure 2b was obtained using a fractional difference filter with $d = 0.9$. The parameter d was gradually increased until the autocovariance plot showed no significant correlations, see Figure 3. The same value of d was effective in removing correlation in all four vertical HRK columns 111108A, 111108B, 111108C, and 121108A (see Figure 1) that formed the basis for our study. A fractional difference filter of order $d = 0.89$ was used in *Lu et al.* [2002] to remove correlations in laboratory ln K data from a vertical sandstone core; a value of $d = 0.9$ was found suitable for a sandstone slab in *Major et al.* [2011] and *Meerschaert et al.* [2004] used $d = 0.74$ for lower resolution ln K values from three horizontal profiles in a sandstone facies at a site in Utah.

[11] The effect of fractional differencing on the histogram is striking. The filtered HRK data in Figure 2b form a coherent shape, with a sharper peak and a heavier tail than a Gaussian (the data fail the Anderson-Darling test for normality, $p < 0.0005$). It is known that correlation can distort a histogram, but we have never seen such a clear example in real data. The fractional difference filter transforms a highly complex histogram into a form amenable to statistical modeling, by removing the correlation. This is the first major finding of our statistical analysis: A simple fractional difference filter is sufficient to capture and remove the correlation structure of a vertical ln K profile. This filter reveals the underlying noise distribution needed to design a faithful ln K field simulation.

[12] The dramatic transformation between Figures 2a and 2b has not been observed previously, perhaps because the available data were either more homogeneous (e.g., laboratory studies of a sandstone slab) or more widely spaced (e.g., flowmeter data from field studies) than the data considered in this study. Since our data are closely spaced, many similar K values tend to clump together due to high correlations, creating histogram peaks. These high correlations are evident in Figure 3a. Mathematically, this strong correlation is a fractional integration. Since each vertical section spans several different facies, with significantly different material properties, multiple peaks can occur in a single HRK profile. The fractional differencing filters out the correlations by reversing the fractional integration.

[13] Next, we discuss our simulation scheme. Since the ln K data exhibit long-range dependence, with a shorter correlation length in the vertical direction, we applied the anisotropic random field generator of *Benson et al.* [2006]: Fourier transformed Gaussian white noise on a 1.5 cm grid was multiplied by a Fourier filter $\psi(\mathbf{k}) = \left[\sum_i C_i |\mathbf{k} \cdot \theta_i|^2\right]^{-(H+1)/2}$ with Hurst index $H = 0.4$, θ_1 horizontal, θ_2 vertical, and correlation length parameters $C_1 = 10$ and $C_2 = 1$ to produce anisotropic ln K fields with a longer correlation length in the horizontal direction. In this simulation, any horizontal row or vertical column of simulated data represents a fractional Brownian motion with Hurst index $H = 0.4$. The horizontal autocorrelation parameter C_1

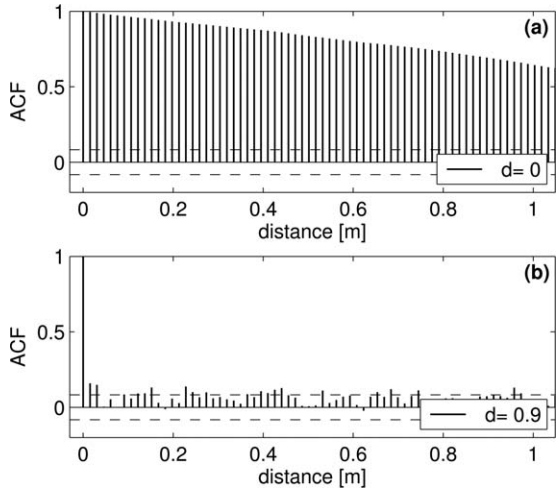

Figure 3. Autocorrelation function for ln K from HRK profile 121108A (see Figure 1) (a) before and (b) after applying the fractional difference filter equation (1) with $d = 0.9$. Autocorrelations inside dashed lines are statistically zero.

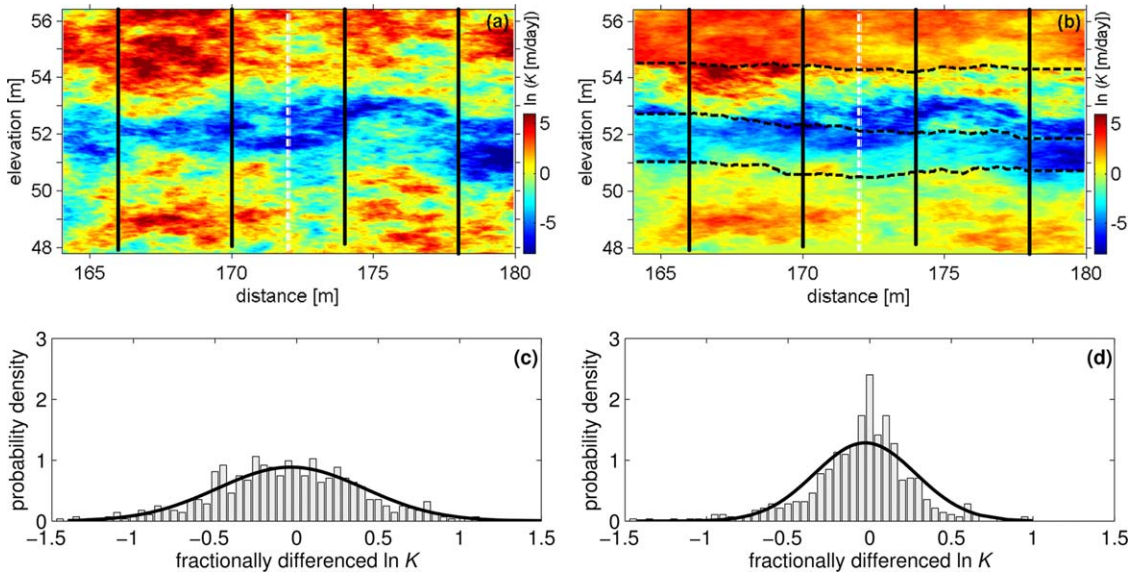

Figure 4. Simulated ln K field (a) without and (b) with GPR facies (dashed lines), conditioned on four HRK profiles (vertical black lines). (c and d) Histogram of one column (white line at $x = 172$ m) from simulated ln K field (a, b, respectively) after applying the fractional difference filter equation (1) with $d = 0.9$. The histogram (Figure 4c) fits a Gaussian model, but the histogram (Figure 4d) from facies simulation (Figure 4b) deviates from Gaussian shape, similar to measured HRK data (Figure 2b).

was chosen to match measured autocorrelations between the four vertical HRK profiles 111108A, 111108B, 111108C, and 121108A used in this study, but due to the 4 m horizontal spacing, this represents only a very rough fit. The simulated ln K field was then adjusted to impose the same mean and standard deviation as the log-transformed HRK data. The conditioning algorithm of *Benson et al*. [2013] was then applied, to make the simulated ln K field agree with available HRK data. Figure 4a shows the results of this simulation procedure for the combined HRK data, without subdividing into GPR facies.

[14] Next, the HRK data were segregated by facies, using the GPR method discussed in section 1. Both the mean and the standard deviation of ln K were found to vary significantly between facies. Separate ln K fields with the same mean and standard deviation as the log-transformed HRK data were generated over the entire model domain for each facies, using the same method of *Benson et al*. [2006, 2013] with the same filter, and the same white noise sequence as in Figure 4a, with dip angle θ_1 matched to the orientation of GPR reflections for each facies. Then, GPR facies boundaries were used to cut out the relevant portions of the simulated ln K field for each facies, resulting in the ln K field shown in Figure 4b. The multiscaling fractal filter used in this simulation methodology produces enhanced connectivity, as compared to a traditional multi-Gaussian model. Connectivity is further enhanced by our facies approach, since ln K statistics vary by facies.

[15] Figure 5 shows the Gaussian fit to fractionally differenced ln K data in a single facies, using the facies boundaries shown in Figure 4b. The data from facies A (shallowest) at horizontal location 174 m had the smallest standard deviation ($\sigma = 0.0110$). The probability plot in Figure 5a shows that these data fit a Gaussian distribution reasonably well, except for a single outlier (0.7244, removed). The histogram (not shown) is similar to Figure 4c. Figure 5b shows the corresponding plot for facies D (deepest) at horizontal location 170 m, which had the largest standard deviation ($\sigma = 0.3637$). Since the points on the probability plot in Figure 5b show a significant and systematic deviation from the reference line, a lack of fit to the Gaussian model is indicated. The histogram (not shown) is similar to Figure 4d. We attribute this deviation from the Gaussian model in our data to the existence of subfacies and smaller sedimentary variations with significantly different material properties [*Dogan et al*., 2011]. In this study, we employ only a few of the most definitive and connected GPR reflection boundaries, to subdivide the model domain into four distinct facies. However, the full geostatistical analysis reported in *Dogan et al*. [2011] did uncover additional substructures. *Zhang et al*. [2013], and others referenced in section 3.5 of that paper, find that subfacies heterogeneity has only a secondary influence on transport, hence the importance of accurately modeling subfacies is unclear.

[16] As noted by *Silliman and Wright* [1988] and further discussed in *Gómez-Hernández and Wen* [1998], a multi-Gaussian simulation with a single covariance function will not produce continuous regions where the highest or lowest ln K values occur. However, in our model, the facies with the highest or lowest mean ln K value produce just such features. This is no contradiction, because our model employs a different multi-Gaussian mean and covariance structure in each facies. In our opinion, the "hole effect" in the variograms of *Rehfeldt et al*. [1992] and *Salamon et al*. [2007] can be the result of combining data from distinct facies, which will naturally cause a deviation from a single multi-Gaussian model with a fixed mean and covariance structure. Furthermore, combining the simulated multi-Gaussian ln K values from different facies does produce the kind of non-Gaussian histogram, with a sharper peak and a heavier tail, frequently seen in column data.

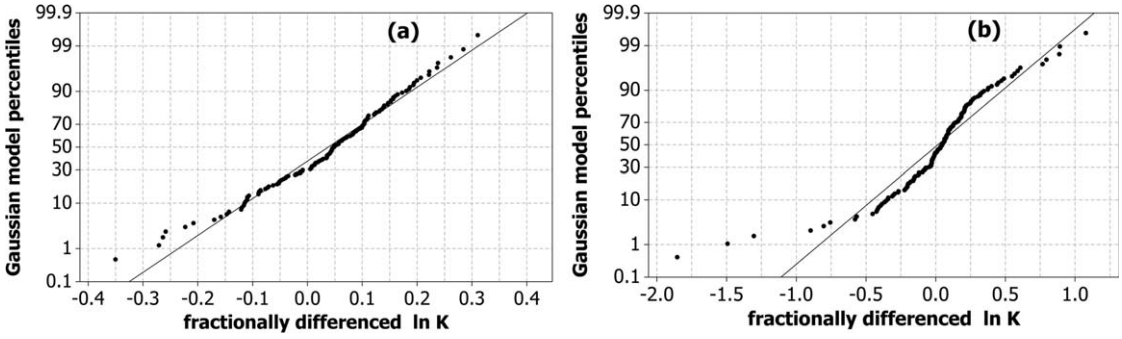

Figure 5. (a) Fractionally differenced ln K data from the shallowest facies at horizontal location 174 m fits a Gaussian distribution. (b) Deepest facies at horizontal location 170 m deviates from the Gaussian model. These probability plots show the sorted data on the horizontal axis, and the corresponding model percentiles for the best fitting Gaussian model on the vertical axis. If the data fits this model, the points will follow the reference line, with some random scatter.

[17] This simulation methodology used to produce the ln K field in Figure 4b produces results similar to the indicator geostatistics method of *Fogg et al*. [1998], which has been successfully applied in both groundwater hydrology [*Weissmann and Fogg*, 1999] and surface water hydrology [*Rubin et al*., 2006]. The idea of combining fractal simulation methods with a facies model is already present in *Lu et al*. [2002]. The difference in our approach is that we use GPR to determine the facies boundaries. Since the actual facies boundaries are known, there is no need to resort to an indicator simulation method to synthesize the facies boundaries. *Ritzi* [2000] notes that lithofacies data can also be used to determine facies boundaries, but if aquifer lithology is not available at sufficient resolution to parameterize a flow and transport model, then a combination of GPR facies and HRK profiles can provide a useful modeling approach for highly detailed K field synthesis.

3. Model Validation

[18] If a simulated ln K profile exhibits the statistical features of a measured ln K data profile, then this validates the simulation methodology. The histogram shown in Figure 4c represents a single column (81st column, at 172 m) of values from the simulated ln K field without GPR facies in Figure 4a, fractionally differenced with $d = 0.9$ as in Figure 2b. Without facies, the fractionally differenced simulated HRK profile fits a Gaussian distribution, and hence does not resemble the measured HRK data. Figure 4d shows the corresponding histogram from a single column of the simulated ln K values with GPR facies in Figure 4b, fractionally differenced with $d = 0.9$. Before fractional differencing, the simulated profile histogram (not shown) appeared similar to Figure 2a. After fractional differencing, the histogram of simulated values in Figure 4d appears quite similar to the corresponding histogram in Figure 2b, with a sharper peak and a heavier tail than the best-fitting Gaussian. There are also some significant differences between Figures 4d and 2b, including a higher peak and some asymmetry in Figure 2b, but the overall shape supports our conclusion that combining simulated Gaussian ln K values from different facies can reproduce a significantly non-Gaussian shape, similar to what is seen in real HRK data profiles. Even though the simulated noise is normal in each facies, the histogram in Figure 4d does not fit a normal probability density (Anderson-Darling test $p < 0.0005$). This is due to the well-known fact that a mixture of Gaussian random variates with different mean and/or standard deviation cannot be normally distributed. Indeed, many non-Gaussian distributions that have been used to model ln K data, including the Laplace and symmetric stable, are Gaussian mixtures [*Kotz et al*., 2001; *Guadagnini et al*., 2012; *Riva et al*., 2013a]. We conclude that GPR facies are useful in this simulation, as they provide a data-based procedure for delineating statistically distinct regions of K values, leading to the more sharply peaked and non-Gaussian profile evident in Figure 4d. The facies approach also allows us to preserve observed correlation structures and angles.

[19] In order to gain a practical appreciation for the accuracy of d estimates, we then simulated a number of statistically identical ln K fields, and applied automatic d estimation to the resulting ln K profiles. Using a standard maximum likelihood estimation routine for fractional autoregressive integrated moving average (ARIMA) models, we found typical estimates of the d parameter to vary from the true (input) value of $d = 0.9$ by ± 0.2 in those simulations. Hence, we cannot rule out other values of d (including $d = 1.0$, a simple difference), and the estimated d value from any single profile should only be taken as a rough indicator of the true value. However, since the value $d = 0.9$ resulted in no significant serial correlation in any of the four HRK profiles in this study, this value was deemed adequate for our purposes. It is certainly possible that more significant variations in d could emerge on a larger scale, or at a different site.

[20] We believe that the departure from a Gaussian distribution, commonly observed in many ln K data profiles from alluvial aquifers, can be attributed to mixing. Although our simulated ln K field is based on Gaussian noise, the distribution of any single column exhibits a significant non-Gaussian shape, because different facies are mixed. This leads to the second major finding of our statistical analysis: A simulation that uses GPR facies, with a fractional Brownian motion within each facies, generates ln K fields whose fractionally differenced vertical profiles have a strongly non-Gaussian distribution, with a sharper

peak and a broader tail, consistent with non-Gaussian ln K models applied in previous studies [*Meerschaert et al*., 2004; *Painter*, 1996]. The GPR data are valuable in this simulation method, since they delineate facies boundaries that allow the Gaussian simulation to reproduce non-Gaussian ln K profiles.

4. Discussion

[21] Modeling and simulation of K fields is challenging, especially in highly heterogeneous aquifers including the MADE site, where the ln K fields exhibit anisotropy [*Boggs et al*., 1990; *Riva et al*., 2008], long-range correlations [*Neuman*, 2003; *Ritzi et al*., 2000], nonmonotone variograms [*Ritzi et al*., 2004; *Salamon et al*., 2007], and a significantly non-Gaussian shape [*Ritzi et al*., 2004]. The standard model of ln K is based on a normal distribution, but many studies have found significant deviations from the Gaussian shape in increments of low resolution ln K field data, with a sharper peak and/or heavier tails [*Meerschaert et al*., 2004; *Painter*, 1996, 2001]. Some researchers have suggested that accurate representation of the K data at the smallest scale may be a critical component of solute transport simulation, particularly regarding the distribution and long-range dependence [*Zheng and Gorelick*, 2003; *Ritzi et al*., 2004; *Dai et al*., 2004; *Ramanathan et al*., 2008]. Based on the statistical analysis reported in this paper, we find that the observed non-Gaussian distribution of fractionally differenced ln K data from alluvial aquifers can be reproduced using a Gaussian ln K field in each facies. The combination of ln K data from different facies at different depths combines into a data profile with a non-Gaussian shape [e.g., *Painter*, 2001]. The non-Gaussian ln K distributions used in previous studies are also Gaussian mixtures of this type. It is well known that mixing of data from different populations changes the histogram shape, but it is usually impossible to reconstruct the Gaussian components. This has led to popular indicator geostatistics methods that synthesize facies boundaries [e.g., *Weissmann and Fogg*, 1999]. Using GPR facies, it does seem possible to delineate the actual facies boundaries without resorting to simulations, and thereby reduce measured ln K data to a reasonably Gaussian form. This allows a simple method for interpolating highly variable and nonstationary ln K fields. Another advantage of facies modeling is laid out in *Winter and Fogg*. [2002, 2003]: It facilitates efficient perturbation-based stochastic methods based on locally homogeneous ln K fields. *Riva et al*. [2013b] has reported a significantly non-Gaussian distribution of log permeability for the two faces parallel to bedding in a relatively homogeneous sandstone slab, while the distribution on the other four faces was close to Gaussian. Hence, the Gaussian facies model promoted here may not be universally applicable.

5. Conclusions

[22] In this paper, ground-penetrating radar (GPR) reflections were used to delineate facies boundaries, and a high-resolution fractal ln K field was simulated within each facies to interpolate between available K data. There were two main findings of this study. First, a fractional difference filter can be useful to capture the correlation structure of ln K profiles. The unfiltered data histogram from one profile is severely distorted, but the filter uncovers a coherent noise distribution, required for simulation design. Second, GPR data can be used to delineate facies boundaries for the K field model. While the overall distribution of ln K profiles in a typical alluvial aquifer deviates significantly from Gaussian, it is reasonable to model the ln K field within each GPR facies as Gaussian. The deviation from Gaussian in the combined profile is the result of mixing, since the combination of data from different Gaussian distributions will no longer fit a Gaussian model. In past research, many investigators have assumed a Gaussian model for ln K, while many others have presented strong evidence for non-Gaussian alternatives. Our analysis indicates that both groups are correct, albeit at different scales, consistent with the findings of *Lu et al*. [2002]. A Gaussian model with an appropriate correlation structure can be adequate for a single facies. For a highly heterogeneous aquifer, comprised of significantly different facies, the combination of ln K values with a different mean and variance in each facies will produce significantly non-Gaussian profiles.

Appendix A: Fractional Difference Filter

[23] The fractional difference filter was pioneered by *Hurst* [1951] to remove correlation in river flood level data. It has now become a standard tool in one-dimensional time series analysis [*Brockwell and Davis*, 1991] and multidimensional spatial statistics [*Beran*, 1994]. Given a correlated time series X_n (or a spatial series collected at equally spaced intervals along a one-dimensional line), the backward shift operator $BX_n = X_{n-1}$ facilitates a simple notation for the fractional difference

$$\Delta^d X_n = (I - B)^d X_n = \sum_{j=0}^{\infty} w_j X_{n-j}, \tag{A1}$$

where the fractional binomial coefficients

$$w_j = (-1)^j \binom{d}{j} = \frac{(-1)^j \Gamma(d+1)}{j!\Gamma(d-j+1)} \tag{A2}$$

using the natural extension of the integer order binomial coefficients. Using the well-known property $\Gamma(x+1) = x\Gamma(x)$ of the gamma function, one can also write

$$w_j = \frac{-d(1-d)\cdots(j-1-d)}{j!} \tag{A3}$$

from which the recursive formula $w_j = w_{j-1}(j-1-d)/j$ follows. Hence in the special case where d is a positive integer, the sum in equation (A1) is finite, since $w_j = 0$ when $j > d$. Integer order derivatives are defined as the limit of difference quotients using these operators. In the same way, fractional derivatives can be defined as the limit of fractional difference quotients [*Meerschaert and Sikorskii*, 2012].

[24] In time series and spatial statistics, an integer order difference is also useful to remove trends, since for example the first-order difference of a linear trend is a constant,

and the second-order difference of a quadratic trend is also a constant. Since the goal is to filter out the correlation (and possibly a trend), an effective fractional difference filter will output an uncorrelated white noise $Z_n = \Delta^d X_n$. This is tested in practice by computing the sample autocorrelation defined by $\hat{\rho}(h) = \hat{\gamma}(h)/\hat{\gamma}(0)$, where the sample autocovariance is defined by

$$\hat{\gamma}(h) = \sum_{n=1}^{N-h} (Z_{n+h} - \overline{Z})(Z_n - \overline{Z}) \quad \text{with} \quad \overline{Z} = \frac{1}{N}\sum_{n=1}^{N} Z_n \quad \text{(A4)}$$

for a data set of length N. Standard statistical theory [*Brockwell and Davis*, 1991] shows that, for large N, the sample autocorrelation of an uncorrelated white noise at any lag h is approximately normally distributed with mean zero and variance $1/N$. Since this random quantity lies between $\pm 1.96/\sqrt{N}$ approximately 95% of the time, the autocorrelation plots in Figure 3 show dashed lines at $\pm 1.96/\sqrt{N}$. Then, the correlation in the data is judged to be statistically insignificant (statistically zero) if 95% of the sample autocorrelations $\hat{\rho}(h)$ lie within these bounds, and the remaining sample correlations do not lie very far outside these bounds. In this case, there is no compelling evidence to contradict the (null) hypothesis that the correlation is zero at any lag $h \neq 0$. The data Z_n in Figure 2b was obtained from equation (1) using the data X_n from Figure 2a, and the optimal value of $d = 0.9$ was determined by increasing d gradually until the autocorrelation (Figure 3) was reduced to be statistically zero. It is also possible to obtain an estimate of d for a single time series using standard maximum likelihood estimation routines for fractional ARIMA models [*Brockwell and Davis*, 1991].

[25] For spatial data in two or three dimensions collected at equally spaced grid points, a fractional difference filter can be applied in each coordinate. The order d of the fractional difference filter can vary with the coordinate to remove spatial correlations. The entire data set can be used to estimate the order(s) of the fractional difference [*Beran*, 1994; *Guo et al*., 2009], which facilitates a more accurate estimate of the d parameter(s).

[26] **Acknowledgments.** Support for this research was provided by NSF grants DMS-1025486, DMS-0803360, EAR-0738938, EAR-0738955, NIH grant R01-EB012079, and PRF grant 48515-G8. Any opinions, findings, and conclusions or recommendations expressed are those of the authors and do not necessarily reflect the views of the funding agencies. We thank Geoff Bohling and Jim Butler at the Kansas Geological Survey for insightful discussions. Thanks also to Hans-Peter Scheffler at the University of Siegen for providing the computer simulation code for operator scaling random fields.

References

Benson, D. A., M. M. Meerschaert, B. Baeumer, and H. P. Scheffler (2006), Aquifer operator-scaling and the effect on solute mixing and dispersion, *Water Resour. Res.*, *42*, W01415, doi:10.1029/2004WR003755.

Benson, D. A., M. M. Meerschaert, and J. Revielle (2013), Fractional calculus in hydrologic modeling: A numerical perspective, *Adv. Water Resour.*, *51*, 479–497, doi:10.1016/j.advwatres.2012.04.005.

Beran, J. (1994), *Statistics for Long-Memory Processes*, Chapman and Hall, Boca Raton, Fla.

Berkowitz, B., A. Cortis, M. Dentz, and H. Scher (2006), Modeling non-Fickian transport in geological formations as a continuous time random walk, *Rev. Geophys.*, *44*, RG2003, doi:10.1029/2005RG000178.

Bianchi, M., C. Zheng, G. R. Tick, and S. M. Gorelick (2011), Investigation of small-scale preferential flow with a forced-gradient tracer test, *Ground Water*, *49*(4), 503–514.

Boggs, J. M., S. C. Young, D. J. Benton, and Y. C. Chung (1990), Hydrogeologic characterization of the MADE site, EPRI EN-6915, research project 2485-5, Interim Rep., Electr. Power Res. Inst., Palo Alto, Calif.

Bohling, G. C., G. Liu, S. J. Knobbe, E. C. Reboulet, D. W. Hyndman, P. Dietrich, and J. J. Butler Jr (2012), Geostatistical analysis of centimeter-scale hydraulic conductivity variations at the MADE site, *Water Resour. Res.*, *48*, W02525, doi:10.1029/2011WR010791.

Brockwell, P. J., and R. A. Davis (1991), *Time Series: Theory and Methods*, 2nd ed., Springer, New York.

Butler, J. J., Jr., P. Dietrich, V. Wittig, and T. Christy (2007), Characterizing hydraulic conductivity with the direct-push permeameter, *Ground Water*, *45*(4), 409–419.

Cushman, J. H., and T. R. Ginn (2000), Fractional advection-dispersion equation: A classical mass balance with convolution-Fickian flux, *Water Resour. Res.*, *36*(12), 3763–3766.

Dai, Z., R. W. Ritzi Jr., C. Huang, Y. N. Rubin, and D. F. Dominic (2004), Transport in heterogeneous sediments with multimodal conductivity and hierarchical organization across scales, *J. Hydrol.*, *294*(1–3), 68–86.

Dogan, M., R. L. Van Dam, G. C. Bohling, J. J. Butler Jr, and D. W. Hyndman (2011), Hydrostratigraphic analysis of the MADE site with full-resolution GPR and direct-push hydraulic profiling, *Geophys. Res. Lett.*, *38*, L06405, doi:10.1029/2010GL046439.

Fogg, G. E., C. D. Noyes, and S. F. Carle (1998), Geologically based model of heterogeneous hydraulic conductivity in an alluvial setting, *Hydrogeol. J.*, *6*(1), 131–143.

Gómez-Hernández, J. J., and X.-H. Wen (1998), To be or not to be multi-Gaussian? A reflection on stochastic hydrogeology, *Adv. Water Resour.*, *21*(1), 47–61.

Guadagnini, A., M. Riva, and S. P. Neuman (2012), Extended power-law scaling of heavy-tailed random air-permeability fields in fractured and sedimentary rocks, *Hydrol. Earth Syst. Sci.*, *16*, 3249–3260, doi:10.5194/hess-16–3249-2012.

Guo, H., C. Y. Lim, and M. M. Meerschaert (2009), Local Whittle estimator for anisotropic random fields, *J. Multivariate Anal.*, *100*(5), 993–1028.

Heinz, J., and T. Aigner (2003), Hierarchical dynamic stratigraphy in various Quaternary gravel deposits, Rhine glacier area (SW Germany): Implications for hydrostratigraphy, *Int. J. Earth Sci.*, *92*(6), 923–938.

Herrick, M. G., D. A. Benson, M. M. Meerschaert, and K. R. McCall (2002), Hydraulic conductivity, velocity, and the order of the fractional dispersion derivative in a highly heterogeneous system, *Water Resour. Res.*, *38*(11), 1227, doi:10.1029/2001WR000914.

Hurst, H. E. (1951), Long-term storage capacity of reservoirs, *Trans. Am. Soc. Civ. Eng.*, *116*, 770–808.

Kohlbecker, M. V., S. W. Wheatcraft, and M. M. Meerschaert (2006), Heavy-tailed log hydraulic conductivity distributions imply heavy-tailed log velocity distributions, *Water Resour. Res.*, *42*, W04411, doi:10.1029/2004WR003815.

Kotz, S., T. J. Kozubowski, and K. Podgorski (2001), *The Laplace Distribution and Generalizations: A Revisit with Applications to Communications, Economics, Engineering, and Finance*, Birkhäuser, Boston.

Liu, G., J. J. Butler Jr., G. C. Bohling, E. Reboulet, S. Knobbe, and D. W. Hyndman (2009), A new method for high-resolution characterization of hydraulic conductivity, *Water Resour. Res.*, *45*, W08202, doi:10.1029/2009WR008319.

Liu, G., C. Zheng, G. R. Tick, J. J. Butler Jr., and S. Gorelick (2010), Relative importance of dispersion and rate-limited mass transfer in highly heterogeneous porous media: Analysis of a new tracer test at the Macrodispersion Experiment (MADE) site, *Water Resour. Res.*, *46*, W03524, doi:10.1029/2009WR008430.

Liu, G., J. J. Butler Jr., E. Reboulet, and S. Knobbe (2012), Hydraulic conductivity profiling with direct-push methods, *Grundwasser*, *17*(1), 19–29.

Llopis-Albert, C., and J. E. Capilla (2009), Gradual conditioning of non-Gaussian transmissivity fields to flow and mass transport data: 3. Application to the Macrodispersion Experiment (MADE-2) site, on Columbus Air Force Base in Mississippi (USA), *J. Hydrol.*, *371*, 75–84.

Lu, S., F. J. Molz, G. E. Fogg, and J. W. Castle (2002), Combining stochastic facies and fractal models for representing natural heterogeneity, *Hydrogeol. J.*, *10*(4), 475–482.

Major, E., D. A. Benson, J. Revielle, H. Ibrahim, A. Dean, R. M. Maxwell, E. Poeter, and M. Dogan (2011), Comparison of Fickian and temporally

nonlocal transport theories over many scales in an exhaustively sampled sandstone slab, *Water Resour. Res.*, *47*, W10519, doi:10.1029/2011WR010857.

Meerschaert, M. M. and A. Sikorskii (2012), *Stochastic Models for Fractional Calculus, De Gruyter Studies in Mathematics 43,* De Gruyter, Berlin.

Meerschaert, M. M., T. J. Kozubowski, F. J. Molz, and S. Lu (2004), Fractional Laplace model for hydraulic conductivity, *Geophys. Res. Lett.*, *31*, L08501, doi:10.1029/2003GL019320.

Molz, F. J., and G. K. Boman (1993), A fractal-based stochastic interpolation scheme in subsurface hydrology, *Water Resour. Res.*, *29*(11), 3769–3774.

Neuman, S. P. (2003), Relationship between juxtaposed, overlapping, and fractal representations of multimodal spatial variability, *Water Resour. Res.*, *39*(8), 1205, doi:10.1029/2002WR001755.

Neuman, S. P., and D. M. Tartakovsky (2009), Perspective on theories of non-Fickian transport in heterogeneous media, *Adv. Water Resour.*, *32*, 670–680.

Painter, S. (1996), Evidence for non-gaussian scaling behavior in heterogeneous sedimentary formations, *Water Resour. Res.*, *32*(5), 1183–1195.

Painter, S. (2001), Flexible scaling model for use in random field simulation of hydraulic conductivity, *Water Resour. Res.*, *37*(5), 1155–1163.

Ramanathan, R., R. W. Ritzi, and C. Huang (2008), Linking hierarchical stratal architecture to plume spreading in a Lagrangian-based transport model, *Water Resour. Res.*, *44*, W04503, doi:10.1029/2007WR006282.

Rehfeldt, K. R., J. M. Boggs, and L. W. Gelhar (1992), Field study of dispersion in a heterogeneous aquifer: 3. Geostatistical analysis of hydraulic conductivity, *Water Resour. Res.*, *28*(12), 3309–3324.

Renard, P., and D. Allard (2011), Connectivity metrics for subsurface flow and transport, *Adv. Water Resour.*, *51*, 168–196.

Ritzi, R. W. (2000), Behavior of indicator variograms and transition probabilities in relation to the variance in lengths of hydrofacies, *Water Resour. Res.*, *36*(11), 3375–3381.

Ritzi, R. W., D. F. Dominic, A. J. Slesers, C. B. Greer, E. C. Reboulet, J. A. Telford, R. W. Masters, C. A. Klohe, J. L. Bogle, and B. P. Means (2000), Comparing statistical models of physical heterogeneity in buried-valley aquifers, *Water Resour. Res.*, *36*(11), 3179–3192.

Ritzi, R. W., Z. Dai, D. F. Dominic, and Y. N. Rubin (2004), Spatial correlation of permeability in cross-stratified sediment with hierarchical architecture, *Water Resour. Res.*, *40*, W03513, doi:10.1029/2003WR002420.

Riva, M., A. Guadagnini, D. Fernàndez-Garcia, X. Sanchez-Vila, and T. Ptak (2008), Relative importance of geostatistical and transport models in describing heavily tailed breakthrough curves at the Lauswiesen site, *J. Contam. Hydrol.*, *101*(1–4), 1–13.

Riva, M., S. P. Neuman, and A. Guadagnini (2013a), Sub-Gaussian model of processes with heavy tailed distributions applied to permeabilities of fractured tuff, *Stochastic Environ. Res. Risk Assess.*, *27*, 195–207, doi:10.1007/s00477-012-0576-y.

Riva, M., S. P. Neuman, A. Guadagnini, and M. Siena (2013b), Anisotropic scaling of Berea sandstone log air permeabilities statistics, *Vadose Zone J.*, doi:10.2136/vzj2012.0153, in press.

Rubin, Y., and A. G. Journel (1991), Simulation of non-Gaussian space random functions for modeling transport in groundwater, *Water Resour. Res.*, *27*, 1711–1721.

Rubin, Y., I. A. Lunt, and J. S. Bridge (2006), Spatial variability in river sediments and its link with river channel geometry, *Water Resour. Res.*, *42*, W06D16, doi:10.1029/2005WR004853.

Salamon, P., D. Fernàndez-Garcia, and J. J. Gómez-Hernández (2007), Modeling tracer transport at the MADE site: The importance of heterogeneity, *Water Resour. Res.*, *43*, W08404, doi:10.1029/2006WR005522.

Schmelzbach, C., J. Tronicke, and P. Dietrich (2011), Three-dimensional hydrostratigraphic models from ground-penetrating radar and direct-push data, *J. Hydrol.*, *398*, 235–245.

Silliman, S. E., and A. L. Wright (1988), Stochastic analysis of paths of high hydraulic conductivity in porous media, *Water Resour. Res. 24*(11), 1901–1910.

Van Overmeeren, R. A. (1998), Radar facies of unconsolidated sediments in the Netherlands: A radar stratigraphy interpretation method for hydrogeology, *J. Appl. Geophys.*, *40*(1), 1–18.

Weissmann, G. S., and G. E. Fogg (1999), Multi-scale alluvial fan heterogeneity modeled with transition probability geostatistics in a sequence stratigraphic framework, *J. Hydrol.*, *226*(1), 48–65.

Winter, C. L., D. M. Tartakovsky, and A. Guadagnini (2002), Numerical solutions of moment equations for flow in heterogeneous composite aquifers, *Water Resour. Res.*, *38*(5), 1055, doi:10.1029/2001WR000222.

Winter, C. L., D. M. Tartakovsky, and A. Guadagnini (2003), Moment differential equations for flow in highly heterogeneous porous media, *Surv. Geophys.*, *24*(1), 81–106.

Zhang, Y., C. T. Green, and G. E. Fogg (2013), The impact of medium architecture of alluvial settings on non-Fickian transport, *Adv. Water Resour.*, *54*, 78–99.

Zheng, C., and S. M. Gorelick (2003), Analysis of solute transport in flow fields influenced by preferential flowpaths at the decimeter scale, *Ground Water*, *41*(2), 142–155.

Zheng, C., M. Bianchi, and S. M. Gorelick (2011), Lessons learned from 25 years of research at the MADE site, *Ground Water*, *49*(5), 649–662.

Zinn, B., and C. F. Harvey (2003), When good statistical models of aquifer heterogeneity go bad: A comparison of flow, dispersion, and mass transfer in connected and multivariate Gaussian hydraulic conductivity fields, *Water Resour. Res.*, *42*(3), 1051, doi:10.1029/2001WR001146.